International Journal of Engineering and Geosciences

https://dergipark.org.tr/en/pub/ijeg

e-ISSN 2548-0960

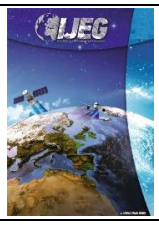

Impact of land use/land cover on land surface temperature and its relationship with spectral indices in Dakahlia Governorate, Egypt

Salem Morsy*[1], Mashaan Hadi[1]

[1]*Cairo University, Faculty of Engineering, Public Works Department, Giza, Egypt*

Keywords
LST
LULC
Spectral indices
Landsat
Regression

ABSTRACT

Land surface temperature (LST) is a direct impact of urbanization and a crucial factor in global climate and land cover changes. In this research, we aim to identify the impact of land use/land cover (LULC) on LST as well as analyze the relationship between LST and three spectral indices using linear, polynomial and multiple regression models. The LST was first retrieved from Landsat imagery using single-channel algorithm. Afterwards, LULC maps were developed using maximum likelihood (ML) classifier and three spectral indices, namely Normalized Difference Vegetation Index (NDVI), Normalized Difference Built-up Index (NDBI) and Normalized Difference Water Index (NDWI). Finally, regression analysis was conducted to model the relationship between LST and the three spectral indices. Landsat 8 OLI/TIRS imagery of year 2019 of Dakahlia Governorate in Egypt was processed for LST retrieval as well as LULC classification. The ML classifier achieved an overall accuracy and kappa coefficient of 95.14% and 0.857, respectively, while of those based on spectral indices were 94.86% and 0.777, respectively. The results demonstrated an average temperature of 35.8°C, 31.2°C and 27.6°C for urban, vegetation and water, respectively. The LST statistics difference between classification methods of the three land covers was less 2°C. Based on the regression analysis, the NDVI and NDWI indicated a negative correlation with LST, while the NDBI indicated a positive correlation with LST. The polynomial regression analysis of LST against NDVI and NDWI demonstrated a better coefficient of determination (R^2) than linear regression analysis of 0.341 and 0.305, respectively. For NDBI, linear and polynomial regression analysis demonstrated very close R^2 of 0.624 and 0.628, respectively. The multiple regression analysis of LST against NDVI, NDBI and NDWI revealed R^2 of 0.699. Consequently, the three spectral indices can be used as effective indicators for separating terrain into different classes, and hence relate their LST.

1. INTRODUCTION

Earth's surface is alerted by extreme modifications caused by human activities, especially the change of land use (i.e., urbanization) (Oke 2002; Arnfield 2003). Urbanization has a great impact on the environment such as changes to cloud cover, temperatures, winds and precipitation (Changnon 1992; Roth 2000; Dousset and Gourmelon 2003; Fan and Sailor 2005). Land surface temperature (LST) is an obvious example on how the urbanization that often takes place rapidly in cities and governorates affects Earth's climate (Oke 2002; Arnfield 2003; Fan and Sailor 2005). This is attributed to a variety of factors. These factors contribute to increase temperatures of the surface or atmosphere in the urban areas, compared to the surrounding environment.

Several studies have been reported on the retrieval of LST from Landsat imagery (Sobrino et al. 2004; Sun et al. 2010; Ibrahim et al. 2019; Sekertekin and Bonafoni 2020). Al-Lami (2015) estimated the LST using Landsat-7 ETM+ imagery of year 2001 for Baghdad city in Iraq. Results showed that the maximum difference of LST between the built-up and the surrounding areas reached to about 12.0°C. The LST was retrieved from Landsat 8 thermal infrared band 10 of year 2015 and compared with the near-air temperature for a part of Ontario and Quebec in Canada (Avdan and Jovanovska 2016). They obtained 2.6°C as an average standard deviation of LST.

* **Corresponding Author**

*(smorsy@eng.cu.edu.eg) ORCID ID 0000-0002-1683-2050
(mashaanhadi@yahoo.com) ORCID ID 0000-0002-0986-3035

Cite this article

Morsy S & Hadi M (2022). Impact of land use/land cover on land surface temperature and its relationship with spectral indices in Dakahlia Governorate, Egypt. International Journal of Engineering and Geosciences, 7(3), 272-282

Research Article / DOI: 10.26833/ijeg.978961

Received: 05/08/2021; Accepted: 21/09/2021

Other studies have been reported on the retrieval of LST and the determination of the relationship between LST, land use/land cover (LULC) and spectral indices (Saleh 2010; Fu and Weng 2016; El-Hattab et al. 2018; Tran et al. 2017; Nse et al. 2020; Guha and Govil 2021). For instance, Fu and Weng (2016) studied the LULC change over the Atlanta metropolitan area and its effect on LST difference. A 507 time series of Landsat imagery from 1984 to 2011 was used. The LULC classification accuracy was 89%, while the change detection accuracy was 92%. Results illustrated that the urban area had the highest mean LST of 21.8°C. El-Hattab et al. (2018) used a neural network approach to develop land cover maps from Landsat TM/ETM+/OLI of the Southern region of Cairo Governorate in Egypt for years 1984, 200 and 2015. They achieved an average overall classification accuracy of 99%. Landsat thermal bands for the same years were used to estimate the LST for the same area. Results showed that urban areas have been expanded from 1984 to 2015; and hence LST increased in those areas.

The impact of LULC on the LST was studied using multi-spectral/multi-temporal satellite data of English Bazar Municipality (Pal and Ziaul 2017). Images from Landsat 5 and Landsat 8 of 1991, 2010 and 2014 were used. Results revealed that LST increased on year basis by about 0.070°C during winter and 0.114°C during summer. LST variations were existed over different LULC types. The built-up area retained highest LST in the studied cases. The relation between LST against NDVI and NDBI was modelled using linear regression, whereas the coefficient of determination (R^2) ranged from 0.441 to 0.62 for NDVI and from 0.470 to 0.607 for NDBI. R^2 for NDBI increased from 1991 to 2014 for winter and summer periods, which establishes the fact that urban areas retain highest LST. However, they reported that the relationship between LST and spectral indices is not always linear (Tran et al. 2017). This is attributed to LULC type, geographic location and season of data acquired.

Dakahlia Governorate in Egypt has documented urban expansion over the past decade due to its accelerated economic growth. This results in a shift of land use from agriculture to other activities such as housing, road construction and industrial activities. All these transformations lead to change in temperatures. This research aims to retrieve the LST of Dakahlia Governorate from Landsat 8 OLI (Operational Land Imager) and TIRS (Thermal Infrared Sensor) imagery of year 2019 and study its relationship with LULC and spectral indices. These indices are the Normalized Difference Vegetation Index (NDVI), the Normalized Difference Built-up Index (NDBI) and the Normalized Difference Water Index (NDWI). This research (1) analyzes the relationship between the LST and the spectral indices using linear, polynomial and multiple regression models, (2) evaluates using spectral indices in land cover classification against widely used supervised classification, maximum likelihood (ML) classifier, and (3) verifies the consistency of LST estimated for LULC extracted based on spectral indices with LST estimated for LULC obtained from ML classifier. The paper is structured as following. Section 2 describes the materials used and methods conducted. Section 3 explains the results and discussion. Section 4 concludes the findings of this research.

2. MATERIALS AND METHODS

2.1. Study Area and Dataset

Dakahlia Governorate, one of the top agricultural production governorates, is located at the northeast of Nile-Delta in Egypt. It covers an area of about 3985.76 km^2 and it extends from 30° 35′ 10″ N to 31° 34′ 02″ N, and from 31° 12′ 47″ E to 32° 07′ 25″ E as shown in Fig. 1 (Abuzaid et al. 2021). It has a population of about 6,697,569 people in 2019 as reported by the Central Agency for Public Mobilization and Statistics. The digital elevation model of the study area, obtained from the Shuttle Radar Topography Mission, varies from zero to 45 m above the sea level as shown in Fig. 2(a). The study area is characterized by a hot dry summer and rainy winter with minimum temperature of 15°C, maximum temperature of 33°C, and a mean temperature of 20°C/year (Abuzaid et al. 2021). The study area earth's physical structure (geology) consists of sand dunes, sabkha-deposits and Nile-deposits (Elnaggar et al. 2020). Dakahlia Governorate is characterized by high density vegetation compared to urban constructions. However, the development of those constructions such as institutions, commercial and industrial buildings and roads network leads to an increase in the anthropogenic activities which in turn alters the natural surface characteristics.

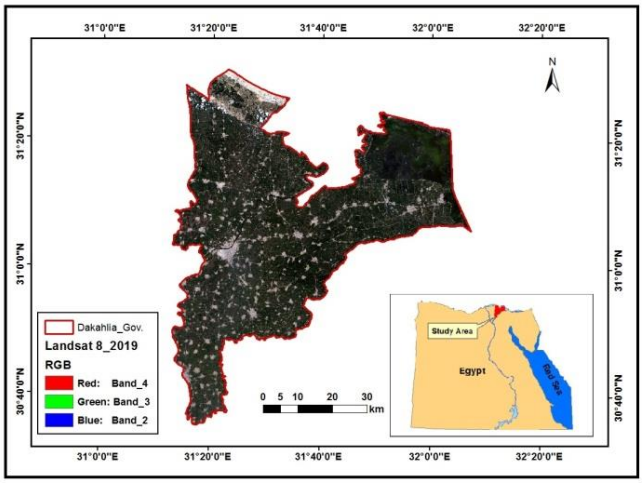

Figure 1. Dakahlia Governorate

The study area was covered by two images from Landsat 8 (path 176, rows 38 and 39) and acquired during the summer season on July 3rd, 2019, Fig. 2(b). The Landsat 8 OLI/TIRS images were downloaded from http://earthexplorer.usgs.gov/. These images are cloud free and consist of eleven spectral bands; eight of them (form 1 to 7 and 9) are 30 m spatial resolution, while band 8 is panchromatic with 15 m spatial resolution. TIRS bands (10 and 11) have 100 m spatial resolution and can be used to obtain surface temperatures. In this research, bands (1 to 7) and thermal band (10) were used.

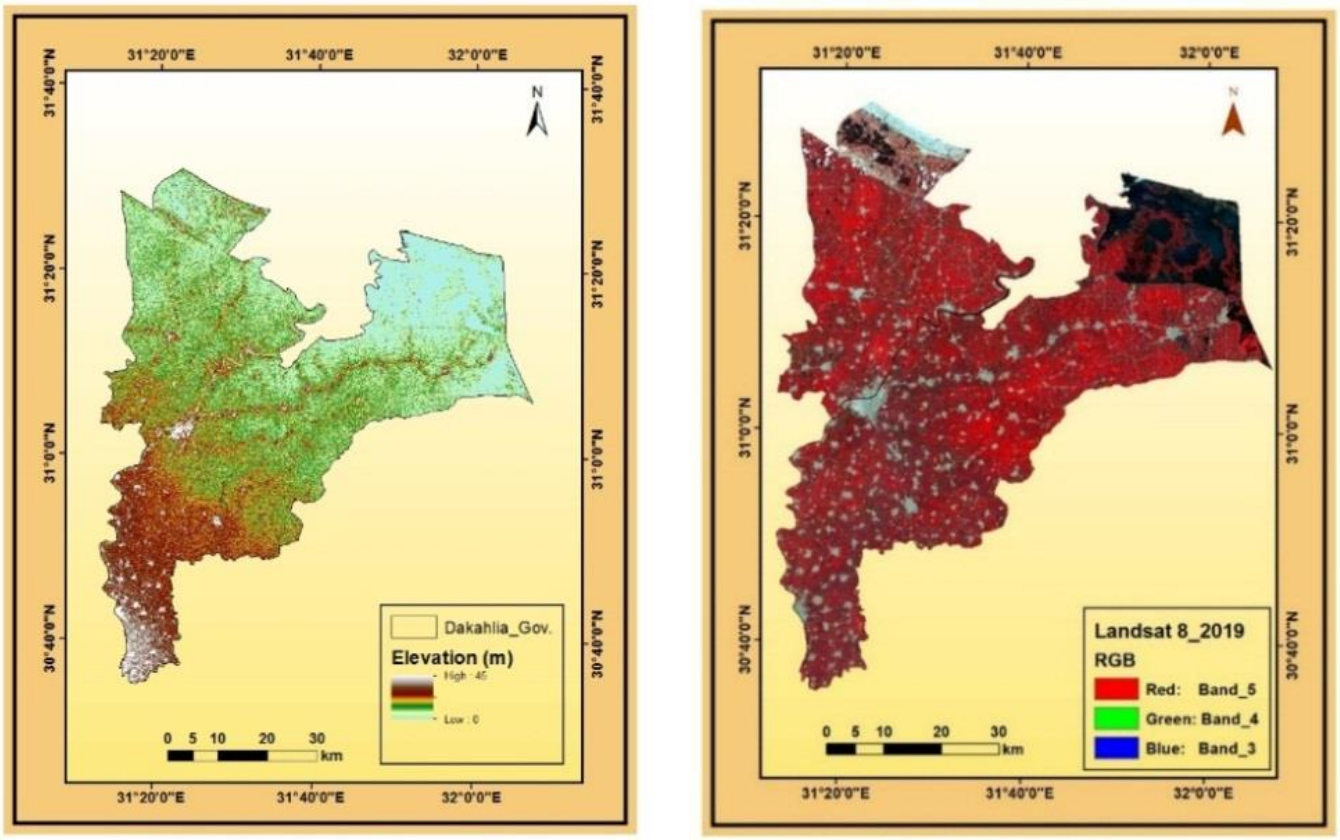

(a) (b)

Figure 2. Landsat images; (a) Digital Elevation Model and (b) False Color Composite

2.2. Overall Work Scheme

Fig. 3 shows the overall workflow of Landsat images processing for LST estimation, spectral indices calculations and supervised image classification. The Landsat images were used to study the LST at different LULC types of Dakahlia Governorate in 2019. The workflow started with atmospheric and radiometric corrections of the images. Then, land cover map was developed and spectral indices, including NDVI, NDBI and NDWI were derived. In parallel, LST was retrieved from band 10 and its relationship with the spectral indices was modelled as explained in the following subsections.

The two images were georeferenced to UTM, Zone 36N, datum WGS 1984 projection. Each OLI/TIRS file was composed of independent single-band images. Firstly, the images were atmospherically and radiometrically corrected using the dark-object subtraction function embedded in ENVI 5.3 software package. Secondly, the ERDAS Imagine 2015 software package was used to resample the images to have the same pixel size (i.e., 30 m). Thirdly, the layer stacking tool was used to combine the single-band images to a multi-band image. Finally, the two images were mosaicked and clipped to form one image covering the study area using a histogram matching and stitching processes.

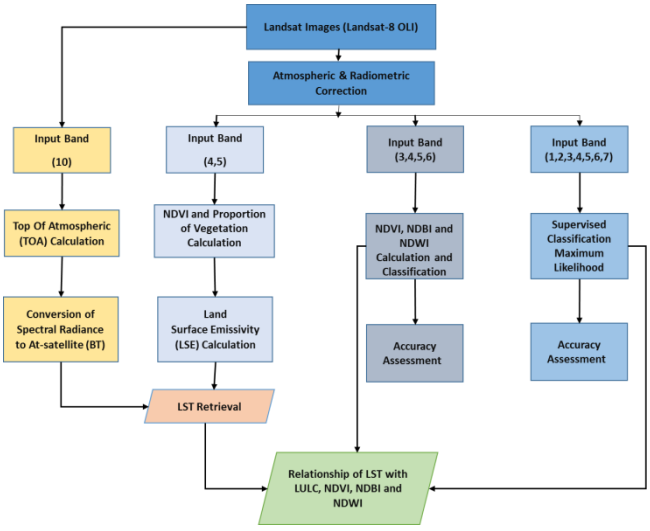

Figure 3. Overall workflow

2.3. Development of the LULC Map

The LULC pattern was mapped using ML supervised classification method including bands from 1 to 7. Four classes were considered for the study area, namely urban, water, vegetation and sand beach. Accuracy assessment was then carried out by compiling a confusion matrix, where a 350 random points were generated over the study area. Accuracy measures (i.e., overall, producer's and user's accuracies) as well as Kappa coefficient were then calculated (Campbell and Wynne 2011).

2.4. Spectral Indices Calculations and Classification

The spectral indices, NDVI, NDBI and NDWI, were derived from the multispectral Landsat imagery. The spectral vegetation, built-up or water index is a single number, between -1 and 1, derived for each pixel from an arithmetic operation on two spectral bands. The reflection from features at different wavelengths is the base of bands selection for any spectral index. A suitable threshold for each index was then identified to distinguish one feature from other land covers (i.e., urban, vegetation or water) based on the spectral characteristics. The Jenks natural breaks optimization method was applied to define a threshold value for each index, and hence separate vegetation, urban and water from NDVI, NDBI and NDWI, respectively.

The NDVI is considered as a measure of healthy green vegetation, and what makes it strong is the use of the highest areas of reflection and absorption of chlorophyll. This index is derived from near infrared (NIR) and red (Red) bands as in Equation 1 (Rouse et al. 1974). The range values of green vegetation are usually from 0.2 to 0.8 (Weng et al. 2004; Avdan and Jovanovska 2016). The NDVI is useful for extracting and mapping vegetation (Chen et al. 2009, MacFaden et al. 2012).

$$NDVI = \frac{NIR - \mathrm{Re}\,d}{NIR + \mathrm{Re}\,d} \tag{1}$$

The reflection of built-up areas in the Short Wave Infrared (SWIR) region is higher than in the NIR region (Zha et al. 2003, Xu 2007). Therefore, the NDBI highlights the build-up areas and can be derived by Equation 2.

$$NDBI = \frac{SWIR - NIR}{SWIR + NIR} \tag{2}$$

McFeeters (1996) defined the NDWI using Green and NIR wavelengths as in Equation 3. The NDWI index was developed for the purpose of using green wavelengths to maximize the reflection of water. As a result, soil and vegetation covers have zero or negative values and thus are suppressed, while the water has positive values which are optimized (McFeeters 1996).

$$NDWI = \frac{Green - NIR}{Green + NIR} \tag{3}$$

In this research, the Jenks breaks optimization method was used to classify all spectral indices. Jenks optimization method or Jenks natural breaks, is designed to increase the deviation between classes and reduce the deviation within-class which represents the best similar values. In another sense, threshold values (breaks) were identified to increase the contrast between classes and reduce it within-class. Consequently, each index was separated into two classes (Chen et al. 2013).

2.5. LST Retrieval from Landsat 8 Imagery

The LST was retrieved using single-channel algorithm developed by (Jiménez-Muñoz et al. 2014) and employed in (Pal and Ziaul 2017, El-Hattab et al. 2018, Salih et al. 2018). Thermal band 10 was used to calculate at-satellite brightness temperature (BT) and land surface emissivity (LSE). Thermal constants of band 10 extracted from the satellite images metadata were required in calculations as provided in Table 1. The LST was retrieved from Landsat images using a series of steps as following.

Table 1. Thermal constant of band 10

Constant	Value
K1	774.885
K2	1321.079
RADIANCE-MULT (M_L)	3.3420E-04
RADIANCE-ADD (A_L)	0.1000

The input of band 10 was used to convert quantized and calibrated digital numbers (Q_{Cal}) to radiation values (L_λ) as indicated in Equation 4, where M_L and A_L are band-specific multiplicative and additive rescaling factors, respectively.

$$L_\lambda = M_L * Q_{Cal} + A_L \tag{4}$$

Afterwards, L_λ was converted to BT using the constants (K1 and K2) of band 10 shown in Table 1 as indicated in Equation 5 (Avdan and Jovanovska 2016).

$$BT = \frac{K2}{Ln\left[\left(\frac{K1}{L_\lambda}\right)+1\right]} \tag{5}$$

Land surface emissivity (Ɛ) was then calculated using as in Equation 6. The Ɛ is a proportionality factor that measures blackbody radiation and predicts the emitted radiation (Salih et al. 2018).

$$\varepsilon = 0.004 * PV + 0.986 \tag{6}$$

Where PV is proportion vegetation and is calculated using the NDVI values ($NDVI_{min}$ and $NDVI_{max}$) using Equation 7 (Salih et al. 2018).

$$PV = \left(\frac{NDVI - NDVI_{\min}}{NDVI_{\max} - NDVI_{\min}}\right)^2 \tag{7}$$

The final step was to retrieve LST using Equation 8 as follows (Salih et al. 2018). LST calculated from

Equation 8 was in Kelvin (K), and it was converted to degree Celsius by subtracting 273.15.

$$LST = \frac{BT}{1 + \lambda * \left(\frac{BT}{P} \right) * Ln(\varepsilon)} \quad (8)$$

Where λ is the radiance wavelength of band 10 (11.5 μm). P is calculated as P= h * c / s, where h is Planck's constant and equals 6.626 * 10^{-34} Js, s is Boltzmann constant and equals 1.38 * 10^{-23} J/K, c is light speed of 2.998 * 10^{8} m/s, and finally P = 1.438 * 10^{-2} m K.

3. RESULTS AND DISCUSSION

3.1. LULC Map Production

The LULC map of the study area was developed from the Landsat imagery using ML classifier. Fig. 4 shows the LULC map, including water, sand beach, vegetation and urban area. It was observed that the highest area was for vegetation representing more than 80% of the total study area, while the sand beach covered the lowest area with less than 2% of the total study area.

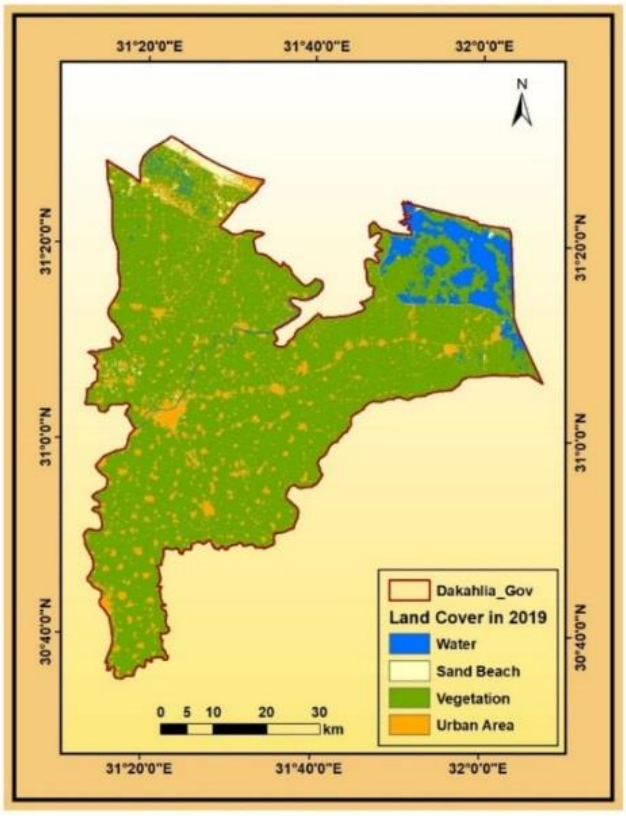

Figure 4. LULC map

The classified image was compared with the actual land use for year 2019. The confusion matrix was computed and accuracy measures (producer's and user's accuracies) were calculated as shown in Table 2. The overall accuracy was 95.14% and Kappa was 0.857. Results showed that the lowest producer's accuracy of 65.38% was for water because many water pixels were wrongly classified as other classes, especially sand beach and vegetation. The lowest user's accuracy was for sand beach (50.00%) because pixels from other classes, especially water and urban, were wrongly classified as sand beach.

Table 2. Producer's and User's accuracies of LULC map.

Class	Producer's Acc. (%)	User's Acc. (%)
Water	65.38	100.00
Sand Beach	100.00	50.00
Vegetation	99.28	97.54
Urban	83.78	93.94

3.2. LULC Based on Spectral Indices Classification

The NDVI, NDBI and NDWI were derived using Equation 1, Equation 2 and Equation 3, respectively. Fig. 5 shows the spatial distribution of three indices. The NDVI map ranged from -1 representing no vegetation area and water bodies to 1 representing high density vegetation area. The vegetation cover has a wide range of NDVI values because it includes different crops and is distributed throughout the study area (Elnaggar et al. 2020). The NDBI values ranged from 1 at area covered by urban area to -1 at no urban cover and water bodies. The NDWI was developed to identify water bodies in remote sensing digital images. The values ranged from 1 at area covered by water to -0.78 at the area of no water.

The Jenks break optimization was then applied to separate land covers from each index. Table 3 provides threshold values based on Jenks break optimization to separate vegetation, urban area and water from NDVI, NDBI and NDWI, respectively. Fig. 6 shows the three classified indices.

Table 3. Threshold values for each index

Index	Class	Threshold
NDVI	Vegetation	≥ 0.3
	Non-vegetation	< 0.3
NDBI	Built-up	≥ - 0.23
	Non-built-up	< - 0.23
NDWI	Water	≥ 0
	Non-water	< 0

Similar to LULC from ML classifier, the classified images, based on spectral indices, were evaluated for year 2019. The confusion matrix was computed for all classes from the three indices and accuracy measures as well as kappa coefficients were calculated as provided in Table 4.

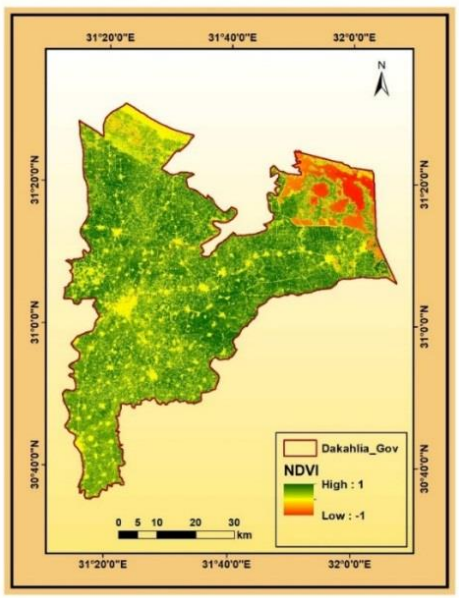

(a)

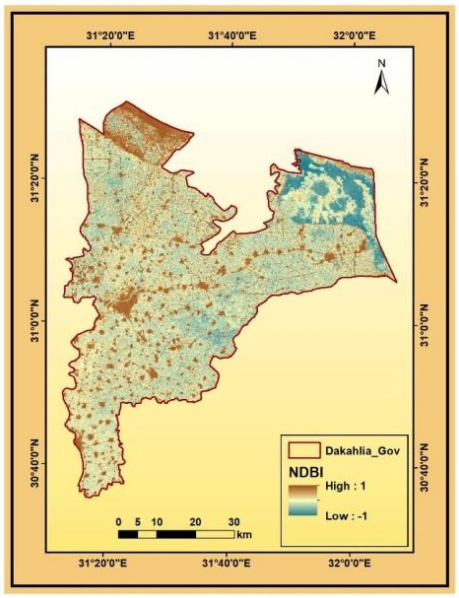

(b)

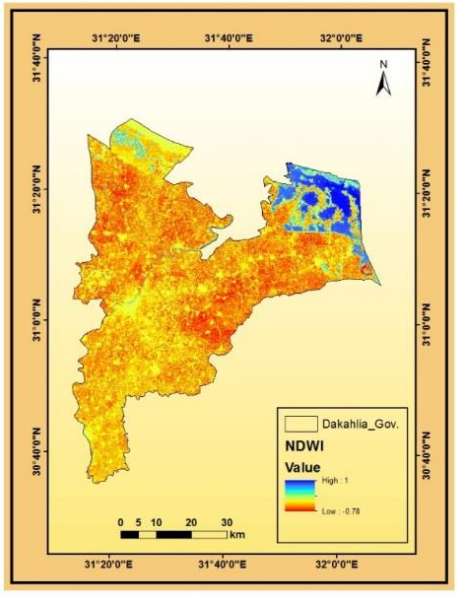

(c)

Figure 5. Spectral indices maps; (a) NDVI, (b) NDBI and (c) NDWI

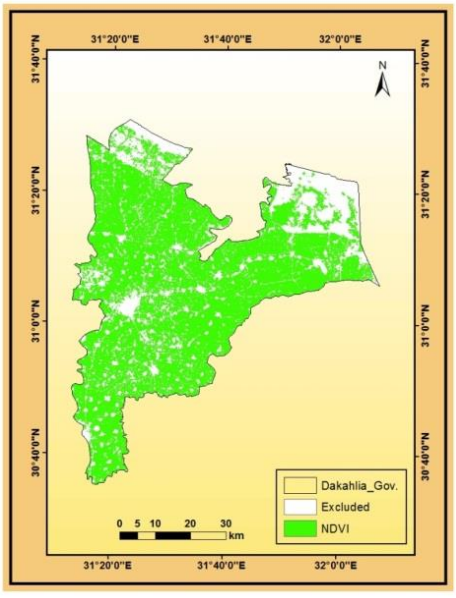

(a)

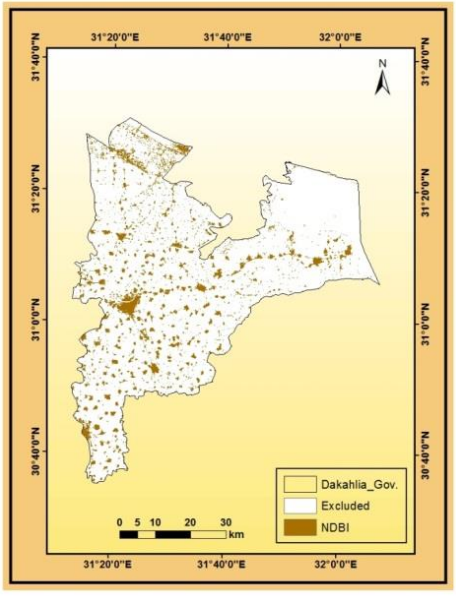

(b)

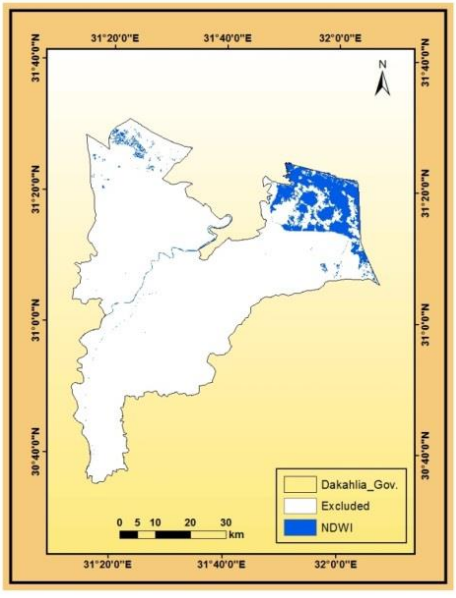

(c)

Figure 6. Spectral indices classes; (a) NDVI, (b) NDBI and (c) NDWI

Table 4. Accuracy measures for classes from spectral indices

Class	Producer's Acc. (%)	User's Acc. (%)	OA (%)	K
Vegetation	90.68	98.44	91.43	0.762
Non-vegetation	94.37	72.04		
Built-up	64.86	85.71	95.14	0.712
Non-built-up	98.72	95.96		
Water	88.46	85.19	98.00	0.857
Non-water	98.77	99.07		

It was observed from Table 4 that the LULC was classified with high accuracy using the three spectral indices. They revealed more than 90% and 0.7 for overall accuracy and Kappa coefficient, respectively. Thus, the use of spectral indices can be directly used for LULC classification without time consuming in training data acquisition as required for ML classifier (i.e., supervised classification).

3.3. LST Retrieval

The LST was retrieved from Landsat thermal band 10 using from Equation 4 to Equation 8. The final LST image is shown in Fig. 7. It was observed from the figure that the lowest temperature of about 27°C was at water and vegetation areas, while the highest temperature of about 46°C was at urban areas. Thus, the modification of natural environment (e.g., vegetation and/or water) with man-made, non-evaporating and non-transpiring structures raised the temperature in the urban development.

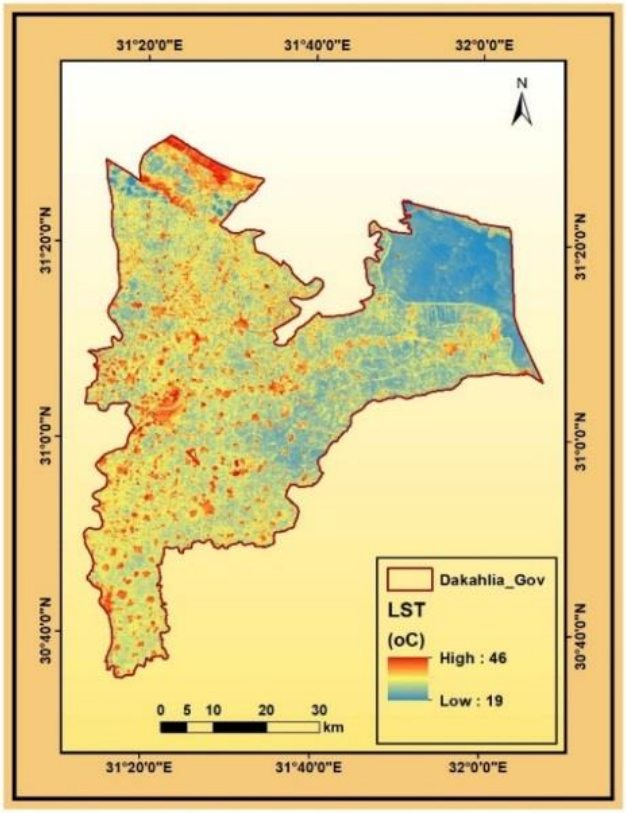

Figure 7. LST map of the study area

3.4. LST, LULC and Spectral Indices Relationship

To estimate the highest and lowest temperatures related to each class; vegetation, urban and water classes were separated from the land cover map in Fig. 5 and then multiplied by the LST map shown in Fig. 7. The LST map for each class is shown in Fig. 8 and the LST statistics related to each class are provided in Table 5. The urban class revealed the highest max, mean and standard deviation temperatures, followed by vegetation and then water cover.

Table 5. LST statistics of LULC based on ML classifier

Class	Min (C°)	Max (C°)	Mean(C°)	SD (C°)
Vegetation	21	43	31.2	2.1
Urban	20	45	35.6	2.2
Water	26	36	27.3	0.8

Similarly, to estimate the highest and lowest temperatures related to each index, the same three classes of vegetation, urban and water resulted from NDVI, NDBI and NDWI, respectably as shown in Fig. 6 were multiplied by the LST map shown in Fig. 7. The LST map for each class is shown in Fig. 9 and the LST statistics related to each class are provided in Table 6.

Table 6. LST statistics of LULC based on spectral indices classification

Class	Min°C	Max °C	Mean°C	SD °C
Vegetation	21	42	31.1	1.9
Urban	20	46	35.9	2.1
Water	25	38	27.6	1.2

Usually, high LST is measured in areas with high NDBI values due to urban constructions. On the other hand, low LST values are measured in areas with higher NDWI values, whereas water bodies have a great role in reducing the radioactive heat flow to Earth's surface. Thus, the radiation energy is consumed through evaporation, which leads to a reduction of LST. Similarly, low LST is measured in areas with high NDVI values, whereas healthy vegetation reduces the effect of Earth's surface temperature.

Generally, we found that the higher LST values are associated with the lower NDVI values. However, few patches of vegetation area in the study area display high temperature variation. This is attributed to the heterogeneity of vegetation coverage (i.e., different crop type and spatial pattern as mentioned in (Elnaggar et al. 2020). In addition, high temperature is associated with urban land (i.e., high NDBI), where densely populated zones and urban constructions are existed. As shown in Fig. 8(c) and Fig. 9(c), inland water bodies display a lower LST than water areas at edges.

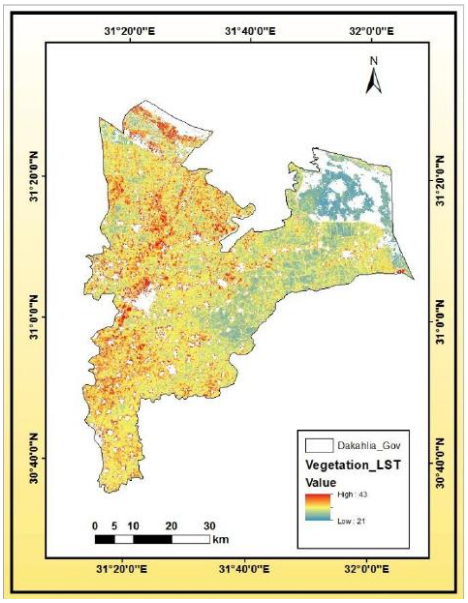

(a)

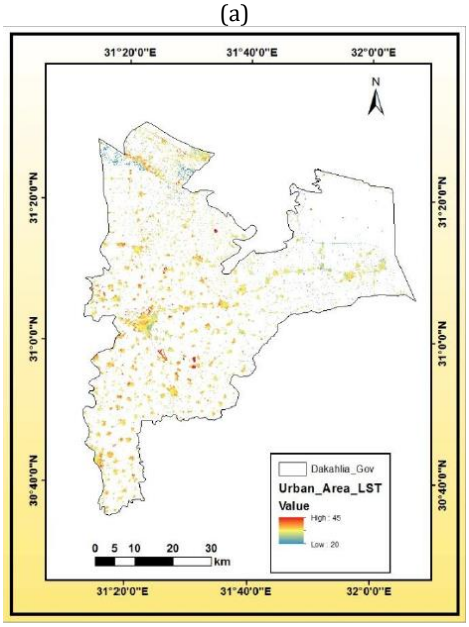

(b)

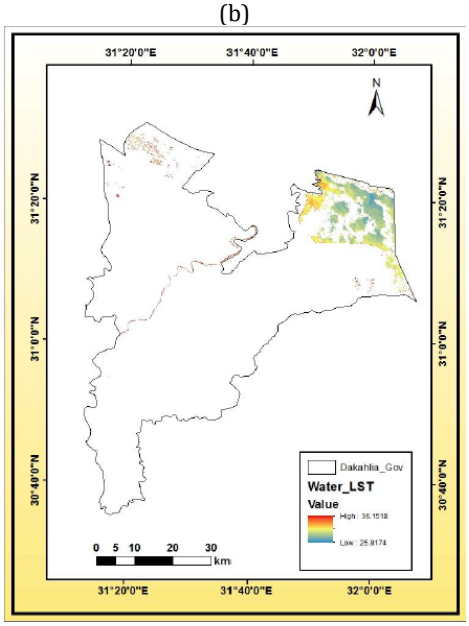

(c)

Figure 8. LST maps for each LULC based on ML classifier; (a) Vegetation, (b) Urban and (c) Water

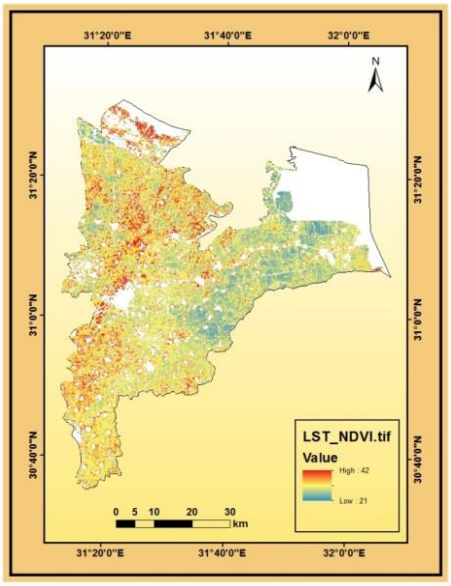

(a)

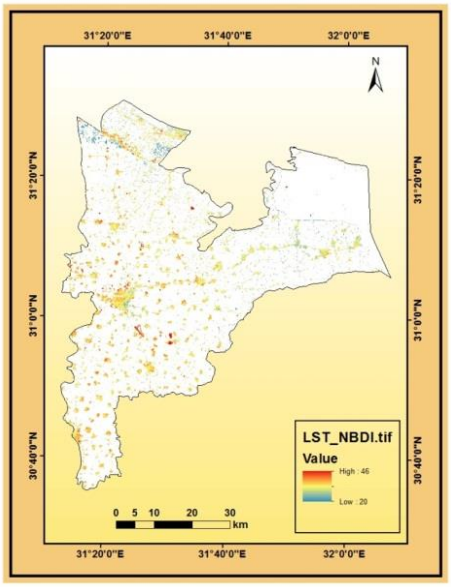

(b)

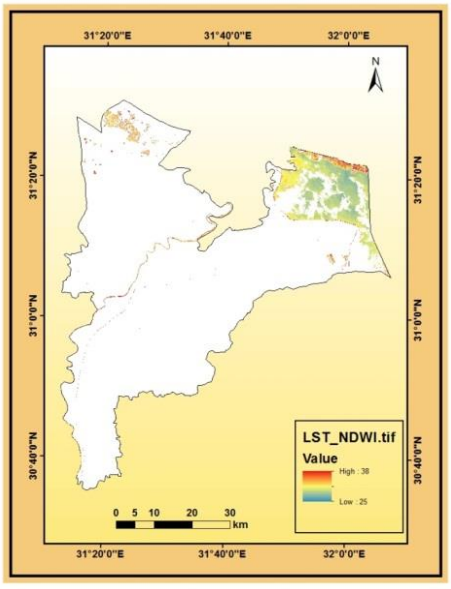

(c)

Figure 9. LST maps for each LULC based on spectral indices classification; (a) Vegetation, (b) Urban and (c) Water

Fig. 10 shows LST statistics comparison for each LULC based on spectral indices classification and ML classifier. LULC based on spectral indices classification have LST statistics close to those of LULC based on ML classifier as shown in Fig. 10. For instance, the max temperatures difference in vegetation and urban are only 1°C, while the min temperatures are the same. For water, the min temperatures difference is only 1°C, while the max temperatures difference is 2°C. All classes have revealed less than 0.5°C difference for the mean and standard deviation. Thus, no significant LST difference was recorded. That means LST can be directly extracted based on spectral indices, whereas spectral indices are effective indicators for the relationship between LULC and LST.

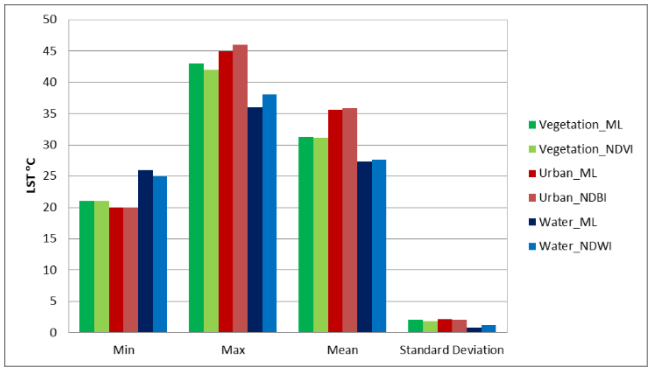

Figure 10. LST comparison for LULC based on spectral indices classification and ML classifier

Consequently, regression analysis was carried out to model the relationship between LST and the three spectral indices. Linear and polynomial regression models were applied for LST against NDVI, NDBI and NDWI as shown in Fig. 11.

The results of regression models indicated a positive correlation between LST and NDBI, while a negative correlation was observed for LST against NDVI and NDWI. The linear regression revealed a low R^2 for NDVI and NDWI of 0.009 and 0.010, respectively, while for NDBI was 0.624. Despite the quite low R^2 related to NDVI or NDWI, the relationship was compatible with previous studies of Pal and Ziaul (2017) and Tran et al. (2017). Polynomial regression models were then carried out to better understand the relationship between LST and the spectral indices. The results showed a higher R^2 for NDVI and NDWI of 0.341 and 0.305, respectively and almost the same R^2 for NDBI of 0.628. Thus, the relationship is not always a linear and could be non-linear as reported by Tran et al. (2017). A multiple regression model was finally developed out for LST against NDVI, NDBI and NDWI and defined as Eq.9:

Equation 9 shows the validity of using spectral indices for LST prediction with R^2 of 0.699 and average absolute residuals of 1.2°C. Thus, the study recommends using NDVI, NDBI and NDWI for terrain classification, LST estimation of terrain classes and prediction of LST in designing and planning urban communities.

$$LST = -21.804\ NDVI + 5.583\ NDBI - 23.214\ NDWI + 34.070 \quad (9)$$

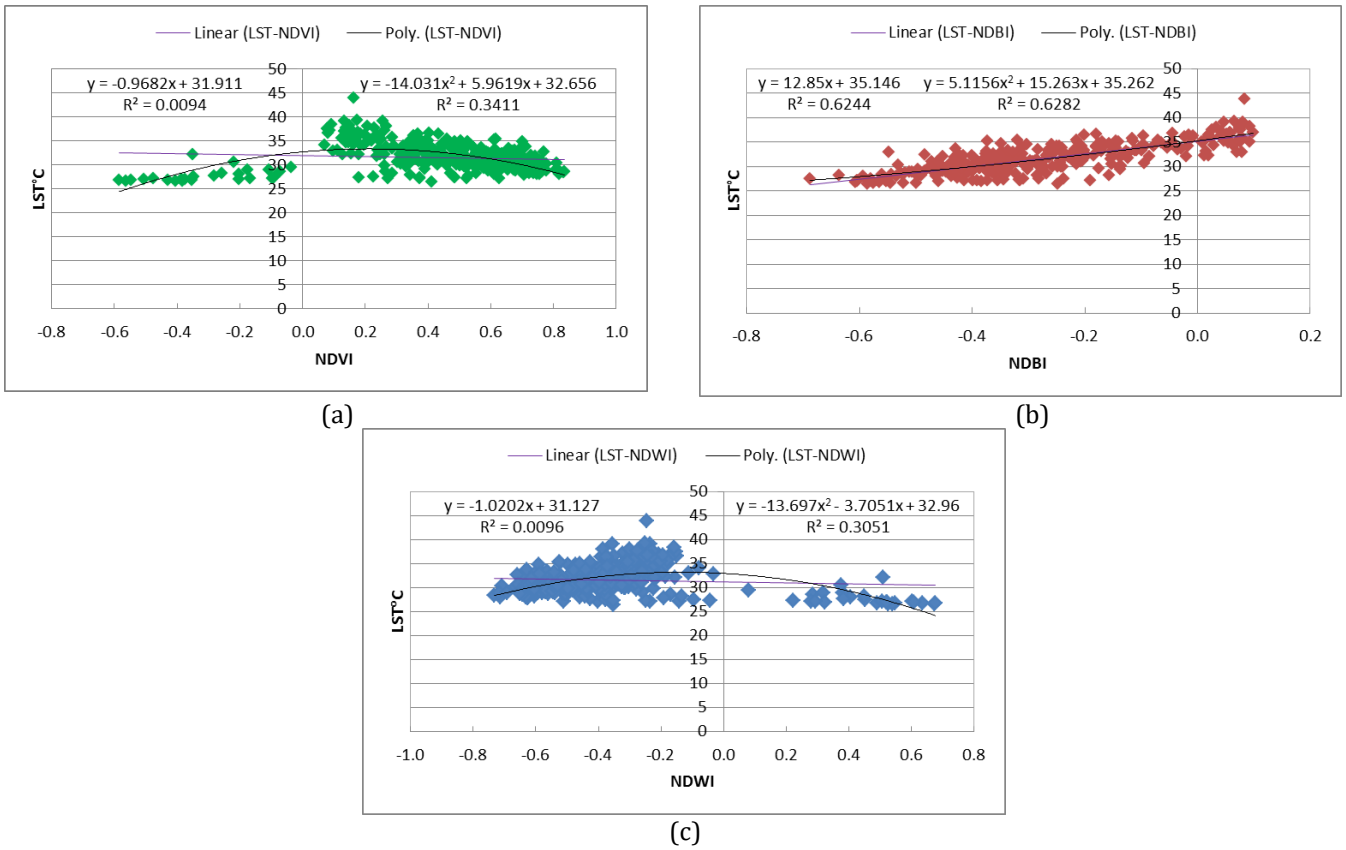

Figure 11. Linear and polynomial regression relationship between LST and (a) NDVI, (b) NDBI and (c) NDWI

4. CONCLUSIONS

In this research, Landsat-8 OLI/TIRS imagery was used to explore the relationship between the LST, LULC and spectral indices of Dakahlia Governorate in Egypt. The LST was retrieved from thermal band 10 and the LULC was developed based on ML classifier and three spectral indices, namely NDVI, NDBI and NDWI. The overall accuracy and kappa coefficient achieved from ML classifier were 95.14% and 0.857, respectively, while the spectral indices achieved an average overall accuracy and kappa coefficient of 94.86% and 0.777, respectively. Thus, unsupervised classification methods (i.e., spectral indices) have achieved comparable results to supervised methods.

Vegetation, urban and water land covers were the focus of this research. Urban cover revealed the max LST statistics based whether on ML classifier or spectral indices with mean value of 35.6°C or 35.9°C, followed by vegetation with 31.2°C or 31.1°C, and then water with 27.3°C or 27.6°C, respectively. It is clearly understood that LST is more in urban area compared to other areas, whereas the temperatures range reached to 25°C or 26°C, based on ML classifier or spectral indices, respectively. The water bodies and vegetation area have a great contribution in reducing the surface temperatures. The LST statistics difference between classification methods of the three land covers vary from less than 0.5°C to 2°C. Thus, using spectral indices is an effective and reliable method in terrain classification, and hence estimating its LST.

Further, linear and polynomial regression was used to model the relationship between LST and spectral indices. A negative relationship was observed for LST against NDVI and NDWI, while NDBI revealed a positive relationship. A multiple regression model was also developed for LST against NDVI, NDBI and NDWI.

Our findings can represent a useful tool for urban designers, planners, architects and policy makers by predicting LST with R^2 of 0.699. It is noted that the relationship is subject to LULC type and geographic location of the study area as well as the season of data acquired.

In this study, we used a traditional supervised classification method (i.e., ML classifier), while recent researches have applied machine learning algorithms in the classification process and achieved better results (e.g., El-Hattab et al. 2018). In addition, monitoring the spatial changes of LULC over time and their impact on LST is necessary for such dynamic study area. Therefore, it is recommended for future work to consider recent machine learning algorithms for LULC classification and explore the relationship between LULC, spectral indices and LST using multi-temporal satellite images.

ACKNOWLEDGMENT

The authors would like to thank the editor and the anonymous reviewers for their valuable comments and suggestions, which helped to improve this work.

Author contributions

Salem Morsy: Conceptualization, Methodology, Software, Validation, Writing-Reviewing and Editing. **Mashaan Hadi:** Data curation, Software, Validation, Visualization, Writing-Original draft preparation.

Conflicts of interest

The authors declare no conflicts of interest.

REFERENCES

Abuzaid A S, Abdellatif A D & Fadl M E (2021). Modeling soil quality in Dakahlia Governorate, Egypt using GIS techniques. The Egyptian Journal of Remote Sensing and Space Science, 24(2), 255-264.

Al-Lami A M (2015). Study of Urban Heat Island Phenomena for Baghdad City using Landsat-7 ETM+ Data. Diyala Journal for Pure Science, 11(2).

Arnfield A J (2003). Two decades of urban climate research: a review of turbulence, exchanges of energy and water, and the urban heat island. International Journal of Climatology: a Journal of the Royal Meteorological Society, 23(1), 1-26.

Avdan U & Jovanovska G (2016). Algorithm for automated mapping of land surface temperature using LANDSAT 8 satellite data. Journal of sensors, 2016.

Campbell J B & Wynne R H (2011). Introduction to remote sensing. Guilford Press. ISBN: 1609181778

Changnon S A (1992). Inadvertent weather modification in urban areas: Lessons for global climate change. Bulletin of the American Meteorological Society, 73(5), 619-627.

Chen J, Yang S, Li H, Zhang B & Lv J (2013). Research on geographical environment unit division based on the method of natural breaks (Jenks). Int. Arch. Photogramm. Remote Sens. Spat. Inf. Sci, 3, 47-50.

Chen Y, Su W, Li J & Sun Z (2009). Hierarchical object oriented classification using very high resolution imagery and LIDAR data over urban areas. Advances in Space Research, 43(7), 1101-1110.

Dousset B & Gourmelon F (2003). Satellite multi-sensor data analysis of urban surface temperatures and landcover. ISPRS journal of photogrammetry and remote sensing, 58(1-2), 43-54.

El-Hattab M, Amany S M & Lamia G E (2018). Monitoring and assessment of urban heat islands over the Southern region of Cairo Governorate, Egypt. The Egyptian Journal of Remote Sensing and Space Science, 21(3), 311-323.

Elnaggar A A, Azeez A A & Mowafy M (2020). Monitoring Spatial and Temporal Changes of Urban Growth in Dakahlia Governorate, Egypt, by Using Remote Sensing and GIS Techniques. (Dept. C. (Public Works)). Bulletin of the Faculty of Engineering. Mansoura University, 39(4), 1-14.

Fan H & Sailor D J (2005). Modeling the impacts of anthropogenic heating on the urban climate of Philadelphia: a comparison of implementations in two PBL schemes. Atmospheric environment, 39(1), 73-84.

Fu P & Weng Q (2016). A time series analysis of urbanization induced land use and land cover change and its impact on land surface temperature with Landsat imagery. Remote sensing of Environment, 175, 205-214.

Guha S & Govil H (2021). Relationship between land surface temperature and normalized difference water index on various land surfaces: A seasonal analysis. International Journal of Engineering and Geosciences, 6(3), 165-173

Ibrahim M S, El-Gammal M I, Shalaby A A, El-Zeiny A M & Rostom N G (2019). Environmental and spatial assessment of urban heat Islands in Qalyubia Governorate, Egypt. Egyptian Journal of Soil Science, 59(2), 157-174.

Jiménez-Muñoz J C, Sobrino J A, Skoković D, Mattar C & Cristóbal J (2014). Land surface temperature retrieval methods from Landsat-8 thermal infrared sensor data. IEEE Geoscience and remote sensing letters, 11(10), 1840-1843.

MacFaden S W, O'Neil-Dunne J P, Royar A R, Lu J W & Rundle A G (2012). High-resolution tree canopy mapping for New York City using LIDAR and object-based image analysis. Journal of Applied Remote Sensing, 6(1), 063567.

McFeeters S K (1996). The use of the Normalized Difference Water Index (NDWI) in the delineation of open water features. International journal of remote sensing, 17(7), 1425-1432.

Nse O U, Okolie C J & Nse V O (2020). Dynamics of land cover, land surface temperature and NDVI in Uyo City, Nigeria. Scientific African, 10, e00599.

Oke T R (2002). Boundary layer climates. Routledge. ISBN: 9781134951338

Pal S & Ziaul S K (2017). Detection of land use and land cover change and land surface temperature in English Bazar urban centre. The Egyptian Journal of Remote Sensing and Space Science, 20(1), 125-145.

Roth M (2000). Review of atmospheric turbulence over cities. Quarterly Journal of the Royal Meteorological Society, 126(564), 941-990.

Rouse J W, Haas R H, Schell J A & Deering D W (1974). Monitoring vegetation systems in the Great Plains with ERTS. NASA special publication, 351(1974), 309.

Saleh S A (2010). Impact of urban expansion on surface temperature Inbaghdad, Iraq using remote sensing and GIS techniques. Al-Nahrain Journal of Science, 13(1), 48-59.

Salih M M, Jasim O Z, Hassoon K I & Abdalkadhum A J (2018). Land surface temperature retrieval from LANDSAT-8 thermal infrared sensor data and validation with infrared thermometer camera. International Journal of Engineering & Technology, 7(4.20), 608-612.

Sekertekin A & Bonafoni S (2020). Land surface temperature retrieval from Landsat 5, 7, and 8 over rural areas: assessment of different retrieval algorithms and emissivity models and toolbox implementation. Remote Sensing, 12(2), 294.

Sobrino J A, Jiménez-Muñoz J C & Paolini L (2004). Land surface temperature retrieval from LANDSAT TM 5. Remote Sensing of environment, 90(4), 434-440.

Sun Q, Tan J & Xu Y (2010). An ERDAS image processing method for retrieving LST and describing urban heat evolution: a case study in the Pearl River Delta Region in South China. Environmental Earth Sciences, 59(5), 1047-1055.

Tran D X, Pla F, Latorre-Carmona P, Myint S W, Caetano M & Kieu H V (2017). Characterizing the relationship between land use land cover change and land surface temperature. ISPRS Journal of Photogrammetry and Remote Sensing, 124, 119-132.

Weng Q, Lu D & Schubring J (2004). Estimation of land surface temperature–vegetation abundance relationship for urban heat island studies. Remote sensing of Environment, 89(4), 467-483.

Xu H (2007). Extraction of urban built-up land features from Landsat imagery using a thematicoriented index combination technique. Photogrammetric Engineering & Remote Sensing, 73(12), 1381-1391.

Zha Y, Gao J & Ni S (2003). Use of normalized difference built-up index in automatically mapping urban areas from TM imagery. International journal of remote sensing, 24(3), 583-594.